Available online at www.sciencedirect.com

jmr&t Journal of Materials Research and Technology

journal homepage: www.elsevier.com/locate/jmrt

Original Article

Surface studies of the chemical environment in gold nanorods supported by X-ray photoelectron spectroscopy (XPS) and *ab initio* calculations

Camila Oliveira [a], *Claudilene Ribeiro Chaves* [b], *Pascal Bargiela* [a], *Maria da Graça Carneiro da Rocha* [a], *Antonio Ferreira da Silva* [c,d], *José Fernando Diniz Chubaci* [c], *Mathias Boström* [e], *Clas Persson* [e,f,**], *Marcos Malta* [a,*]

[a] *Instituto de Química, Departamento de Físico-Química, Universidade Federal da Bahia, Campus Ondina, Salvador, BA, Brazil*

[b] *Rede Multidisciplinar de Pesquisa, Ciência e Tecnologia, Universidade Federal de Uberlândia, Campus Patos de Minas, Patos de Minas, MG, Brazil*

[c] *Instituto de Física, Universidade de São Paulo, Laboratório de Cristais Iônicos, Filmes Finos e Datação, Butantã, São Paulo, SP, Brazil*

[d] *Instituto de Física, Universidade Federal da Bahia, Campus Ondina, Salvador, BA, Brazil*

[e] *Centre for Materials Science and Nanotechnology, Department of Physics, University of Oslo, NO-0316, Oslo, Norway*

[f] *Department of Materials Science and Engineering, KTH Royal Institute of Technology, Stockholm, SE, 100 44, Sweden*

ARTICLE INFO

Article history:
Received 14 May 2021
Accepted 14 August 2021
Available online 21 August 2021

Keywords:
Gold nanorods
X-ray photoelectron spectroscopy (XPS)
nanoparticles
Simulation
ab initio

ABSTRACT

In this manuscript, we prepared gold nanorods (Au-NRs) through "silver-assisted seeded methodology" and studied their outermost layer using XPS spectroscopy and *ab initio* calculations to compare the chemical states of the constituents of the metallic core. Supporting first-principles calculations employing a relativistic, full-potential and all-electron method, with augmented plane waves plus local orbitals as a basis set, ensure proper treatment of the core electron states. Three significant findings can be reported. First, we found that besides Au (0), there are two chemical states for silver, namely Ag (0) and Ag(I), on the Au surface. Our results corroborate with recent results reported in the literature, indicating that Ag monolayer can be oxidized to Ag(I) during the steps of centrifugation and washing with diluted CTAB solution. Second, *ab initio* simulations showed that Ag atoms have different binding energies, depending on their configuration in Au-NRs (whether silver atoms are found on the surface or if they are spread in bulk as interstitial or substitutional defects). Third, theoretical studies showed that silver atoms located at

* Corresponding author.
** Corresponding author.
E-mail addresses: clas.persson@fys.uio.no (C. Persson), marcosmalta@ufba.br (M. Malta).

https://doi.org/10.1016/j.jmrt.2021.08.059

interstitial sites could distort the crystalline structure, and, therefore, we do not expect interstitial Ag to occur in Au-NRs.

1. Introduction

Noble metal nanostructures have been the subject of significant research in recent years. The interest in these materials is derived from new physicochemical properties achieved at the nanoscale, such as variable optoelectronic properties or maximization of the surface-to-volume ratio [1,2]. Usually, metallic nanoparticles are obtained by treating metal salts with reducing agents in a medium containing capping ligands that bind to the metal surface [3]. The capping ligands are crucial in forming and stabilizing nanoparticles because they prevent disordered growth and avoid agglomeration [4].

Gold nanorods (Au-NRs) are intriguing nanostructures that have attracted much attention due to plasmonic optical properties, which are very sensitive to their aspect ratio (i.e., length/diameter), dispersion, and homogeneity [5,6]. Localized surface plasmon resonance (LSPR) originates from the interaction between an incident electromagnetic radiation with free electrons on the metallic surface [7]. When the wavelength of light is much larger than nanoparticle size, the electromagnetic field of the light induces a collective oscillation of the free electrons relative to the lattice of positive nuclei. As a result, Au-NRs will exhibit intense light absorption and scattering at specific resonant wavelengths, depending on the aspect ratio and dielectric environment [8]. Besides, Au-NRs can release heat to the media through exposure to near-infrared radiation (NIR) [9]. These characteristics make Au-NRs promising for various applications such as bioanalytical essays, biomedical imaging, drug delivery, and photothermal therapy [5]. Single Au-NR can be modeled as an elongated inorganic particle (i.e., distinct length and diameter dimensions) surrounded by a dense layer of organic molecules, generally cetyltrimethylammonium bromide (CTAB). It is essential to notice that while the inorganic particle is found in the nanoscale, with behavior and properties inherent to this size regime, the organic ligand affects the particle itself [10]. For instance, studies have shown that CTAB exerts toxic effects on the cells. Thus, it makes necessary to replace CTAB with another biocompatible shell such as thiolated polyethylene glycol (PEG-SH) before *in vivo* applications of Au-NRs [11,12].

Currently, the "silver-assisted seeded methodology" is the most popular route to obtain Au-NRs in considerably high yields. The synthesis is divided into two steps: firstly, CTAB capping Au seeds with an average diameter of 2.0 nm are prepared through reduction with sodium borohydride. In the second step, the Au seeds are added to a growth solution containing $HAuCl_4$, CTAB, $AgNO_3$, and a mild reducing agent such as ascorbic acid. The final morphology concerning dimensions and aspect ratio can be regulated by varying the concentration of silver nitrate [13,14].

Despite considerable advances in understanding the processes of synthesis and formation of Au-NRs, the constitution of the metallic core is still a point of scientific controversy [15,16]. For example, in single-crystal rods obtained by "seed methodology", there is still a debate regarding the role of Ag in the composition and structure of the metallic core. Two hypotheses describe the role of Ag depending on the oxidation state of deposited silver, whether Ag(0) or Ag(I). For the case of Ag(I), it is supposed that silver ions may form a complex with Bromine on particular surface facets, preventing growth on these facets [17,18]. In a second hypothesis, Ag(I) is preferentially reduced onto higher energy surface facets of gold through underpotential deposition (UPD), forming an Ag(0) monolayer on the nanorods. More recently, Moreau and coworkers proposed a new mechanism regarding the role of trace Ag in the synthesis of Au nanorods. Accordingly, Ag participates in the anisotropy of structure because it deposits initially on the Au surface, making the length growth rate exceeds the diameter growth rate. However, as the reaction evolutes, Ag is progressively incorporated into the bulk of the nanorods due to the subsequent deposition of gold atoms. According to this proposal, in the final stages of the reaction, most surface atoms are Au [15].

Here, we report our findings on the surface characterization of Au-NRs using X-ray photoelectron spectroscopy (XPS) to access the outermost layer of the metallic core. To complement information regarding the contribution of different Ag species on Au-NRs by experimental XPS, we carried out *ab initio* calculations to simulate the chemical state of the metallic core. Thus, based on XPS experimental data, we compare the values of binding energy (BE) of the Au and Ag components with the theoretical acquisition of BE using the WIEN2k/VASP package. Important to note that computational support was substantially simplified, considering only the metallic core and the atoms behaving as in bulk. Small clusters with approximately 50 metal atoms behave like large molecules, while large ones with 300 or more atoms exhibit characteristics of a bulk sample [19]. The main results regarding the chemical environment of the metallic core of Au-NRs obtained by "silver-assisted seeded methodology" are presented below. Our results also suggest that silver coexists on the outermost surface in two oxidation states, namely Ag^0 and Ag^+, in addition to metallic gold.

2. Experimental and theory

Hydrogen tetrachloroaurate ($HAuCl_4.3H_2O$, 99.999%), cetyltrimethylammonium bromide (CTAB, > 98.0%), sodium borohydride ($NaBH_4$), and ascorbic acid were purchased from Aldrich. Silver nitrate ($AgNO_3$, 99.999%) was obtained from Merck. All chemicals were used as received without further purification. Samples were prepared using deionized water

(Millipore Milli-Q Water System), and whole glassware was previously cleaned using aqua regia solution (3:1 HCl/HNO_3). Caution: aqua regia is a highly oxidizing solution and must be handled with extreme care.

The synthetic route of preparing Au-NRs was based on a two-step seed-mediate process following the methodology described by Nikoobakht and El-Sayed [13]. Firstly, Au seeds were synthesized by adding 5.0 mL of a 0.5 mmol L^{-1} solution of $HAuCl_4$ in 5.0 mL of a 200.0 mmol L^{-1} solution of CTAB. Next, 600 μL of 10.0 mmol L^{-1} of an ice-cold $NaBH_4$ was added under vigorous agitation for 3 min. In the second part, Au-NRs were prepared by adding 1.0 mmol of CTAB in 5.0 mL of deionized water at 27–30 °C. Then, sequentially it was added 100 μL of 4.0 mmol L^{-1} of $AgNO_3$, 5.0 mL of 1.0 mmol L^{-1} of $HAuCl_4$, and 100 μL ascorbic acid 78.8 mmol L^{-1}. Finally, 12 μL of the seed solution was gently added, resting it on the liquid surface and keep undisturbed for about 12 h.

The absorbance spectrum of the solution containing Au-NRs was acquired over a range from 350 to 1000 nm using a UV–Vis Rigol Ultra-3560 spectrophotometer. The particle morphologies were analyzed using a Transmission Electron Microscopy Tecnai G2-12- SpiritBiotwin FEI - 120 kV from UFMG Electronic Microscopy Center. X-ray photoelectron spectroscopy (XPS) was carried out using a Kratos Axis Ultra DLD using a monochromatic Al Kα (1486.6 eV) X-ray source, 150 W, 10 mA and 15 kV. The survey spectrum was recorded with a pass energy of 80 eV and 1 eV per step, and high-resolution spectra were recorded with a pass energy of 40 eV and 0.1 eV per step. The binding energy (BE) of the core level C 1s set at 284.8 eV was used for spectra calibration to compensate for surface-charging effects. The elemental relative sensitivity factors (RSF) provided by the instrument's manufacturer were used for elemental quantification. Casa XPS (version 2.3.17) was employed for data treatment. For sample preparation, Au-NRs were separated by centrifugation, then washed with diluted CTAB solution to remove the excess of surfactant and unreacted gold and silver and separated again by centrifugation. The detailed procedure for this treatment is presented as follow: as-prepared Au-NRs solutions were centrifuged for 2:30 h at 2000 rpm; after deposition of the nanoparticles on the bottom of the centrifuge tube, the supernatant was removed and subsequently 10 mL of diluted 1.0 mmol L^{-1} of CTAB solution was added, homogenized and centrifuged again at 3000 rpm for at least at 2 h. After removal of the supernatant, samples were transferred to an Eppendorf vial and dried by lyophilization.

The theoretical modeling of gold crystal was analyzed within the density functional theory (DFT), employing the Kohn–Sham equation and using the all-electron augmented plane wave method with local orbitals as provided in the WIEN2k package version 18.2 [20]. Bulk gold structures, either defect-free or with Ag as defect were described by unit cells of $3 \times 3 \times 3$ primitive cells. Atom configuration of Au was $[Xe]:4f^{14}|_{core}\ 5d^{10}6s^{1}|_{val}$ and configuration of Ag was $[Kr]:|_{core}\ 4d^{10}5s^{1}|_{val}$, where the subscripts indicate if the orbitals are treated as fully-relativistic core states or as valence states for which the spin-orbit coupling is neglected. The experimental lattice constant $a = 4.0782$ Å was used, and the ionic relaxation was performed with VASP until forces on the atoms were smaller than 8.0 meV/Å [21,22]. For these metallic systems, the Perdew–Burke–Ernzerhof (PBE) exchange-correlation functional was chosen. The energy cutoff was determined by $R_{mt} \cdot K_{max} = 8$, with the muffin-tin radius of $R_{mt} = 1.2$ Å. The wavefunctions were constructed with maximum azimuthal number $l = 12$ inside atomic spheres and with non-muffin-tin matrix elements up to $l = 6$. Silver defects in gold bulk structures were modeled with $3 \times 3 \times 3$ face-centered primitive cells. Silver surface adatom was described by an atom at the three-fold hollow site of the Au [111] surface modeled with a trilayer of 3×3 hexagonal primitive cells. Since metals require a reasonably accurate Fermi level, we used a **k**-meshes of $20 \times 20 \times M$ grid with $M = 20$ for bulk and $M = 1$ for the layer structure. The binding energies were calculated utilizing the Slater transition theory with ½ electron excitation to vacuum, compensated by a corresponding background charge. For more details about the computational model, check the Electronic Supplementary Information (ESI).

3. Results and discussion

Although Au-NRs obtained by "seed methodology" have been extensively studied since the initial works of Murphy and El-Sayed groups [13,23,24], the chemical environment of the metallic core still generates debate in the scientific community. The modeling and characterization of this material class (and other types of gold nanostructures) is challenging because the modification of few experimental parameters, such as the ratio of reactants and temperature of synthesis, can lead to products with very distinct morphological characteristics [25–27]. Additionally, chemical models are puzzling and often contrasting each other because the structure of Au-NRs is elucidated in diverse media and using different experimental tools, such as ultraviolet–visible spectroscopy (UV–Vis), nuclear magnetic resonance (NMR), X-ray photoelectron spectroscopy (XPS), transmission electrons microscopy (TEM) or surface-assisted laser desorption/ionization (SALDI-MS) and, therefore, a reliable figure of the system is still sought [17,18,28]. Our research was motivated by recent works published in the literature showing two different proposals for the chemical state of silver in gold nanorods: first, the suggestion of Moreau and co-workers [15] reporting the internalization of Ag atoms into Au crystal during the growth of nanorods; the second proposal was elaborated by Ye et al. [16] suggesting the oxidation of silver surface monolayer due to the desorption of the CTAB molecules when the nanoparticles are rinsed with water or ethanol. In this manuscript, XPS was used to determine the surface chemistry of the outermost layer of Au-NRs in parallel with *ab initio* calculations to increment information about the binding energy of silver atoms (Ag^0) in different configurations (or chemical states) in gold crystals. The simulated systems were bulk gold, either defect-free or with Ag as a defect (Ag-on-Au site, i.e., substitutional defect, and Ag interstitial defect in Au crystal) and silver surface adatom over Au crystal.

Fig. 1a shows a typical UV–Vis–NIR spectrum and the corresponding transmission electron micrography of Au-NRs prepared by seed-methodology. As expected, the image shows the Au-NRs absorption profile, which presents two

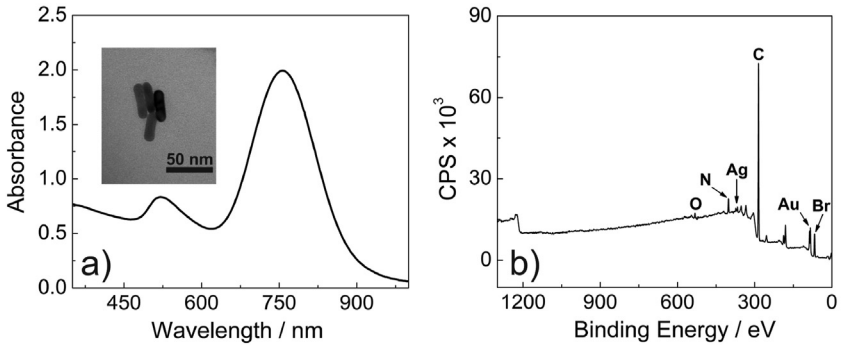

Fig. 1 – (a) UV–Vis–NIR spectrum of an aqueous solution containing CTAB-capped Au-NRs. Inset: TEM micrography of typical Au-NRs. (b) XPS survey spectrum of the Au-NRs.

distinct plasmon bands associated with the anisotropy in the structure: one corresponding to the transverse band (short axis) at 520 nm and one corresponding to the longitudinal band (long axis) at 757 nm. TEM micrography presented in the inset of Fig. 1 shows the typical rod-like structure of these NPs. The nanoparticles aspect ratio was estimated to be 3.5 from the UV–Vis spectrum presented in Fig. 1a (check ESI for details) [29–31]. XPS is a powerful technique for characterization and determination of surface chemistries of the (nano)materials. Owing to the inelastic scattering of the electrons in the analyzed sample, the information obtained is regarding only to the outermost surface layer in the range of 5–10 nm [32]. Analysis of the surface layer using XPS has been conducted to the speciation of organic components and the metallic core of Au-NRs. The wide scan XPS spectrum is presented in Fig. 1b. As expected, it was detected the signals corresponding to carbon, nitrogen, Bromine, gold and silver. These elements are the chemical constituents of the CTAB bilayer and the metallic core. Important to notice, it was not observed the signals corresponding to chlorine in the sample, indicating that centrifugation and redispersion of Au-NRs in 1.0 mmol L^{-1} CTAB solution was efficient in removing the excess of CTAB and reactants in the samples. Additionally, the presence of oxygen was observed. The oxygen is assigned to the presence of adventitious carbonaceous compounds due to sample handling under environmental conditions [33]. The high-resolution spectra in the regions of the C 1s, N 1s, Br 3d, O 1s, Ag 3d and Au 4f were registered in order to determine the atomic concentrations (%) and binding energies (eV) of the elements.

Table 1 presents the surface composition of Au-NRs in terms of relative atomic concentration (%) and binding energies (eV) determined by XPS. The components of the cationic surfactant C, N and Br, presented atomic concentrations of 91.01, 3.77 and 3.11%, respectively. Oxygen was observed in an atomic concentration of 0.83%. The metal concentrations of Au and Ag are 1.07 and 0.21%, respectively. The calculus of the percentage of silver compared to gold is approximately 16% of the metallic layer. This value is considerably higher than that found by Liz-Marzán and co-workers in a former XPS study (around 9% of silver) [34]. Previous inductively couple plasma spectroscopic (ICP) experiments carried out by Orendorff and Murphy found values of silver percentage ranging from 2.5 to 4.5% of total metal concentration in nanorods [35]. The reason for this difference in the amount of silver is still unclear. However, given the complexity of the medium, with several reactions co-occurring and several parameters that affect the final product (such as temperature, pH and the ratio between reagents), it may cause some lack of reproducibility between the final products [36].

Table 1 – Surface chemical composition of Au-NRs as obtained by high-resolution XPS spectra.

Element regions	Peak-Binding energy (eV)	Suggested attributions	Surface concentration (at. %)	Total (%)
C 1s	284.8	C–H, C–C (C1)	63.2	91.0
	285.6	C–N (C2)	19.6	
	286.3	$-N-(CH_3)_3$ (C3)	6.9	
	287.8	$C_{adv} = O$ (C4)	1.3	
N 1s	402.1	$-N^+$	3.8	3.8
Br $3d_{5/2}$	67.0	Br^-	1.8	3.1
Br $3d_{3/2}$	68.1		1.3	
O 1s	532.1	C–O	0.8	0.8
Au $4f_{7/2}$	83.5	Au(0)	1.1	1.1
Au $4f_{5/2}$	87.2			
Ag $3d_{5/2}$	368.2	Ag(0)	0.03	0.2
Ag $3d_{3/2}$	374.3			
Ag $3d_{5/2}$	367.4	Ag(I)	0.2	
Ag $3d_{3/2}$	373.4			
				100.0

A large amount of silver in the rods can be rationalize considering three different mechanisms of growth summarized by Lohse and Murphy [37]. In the first mechanism, it supposed that a silver(I) bromide complex ($AgBr_2^-$ or CTA–Br–Ag^+) blocks the gold surface in the longitudinal facets, favoring the anisotropic growth of the rods. That is, the silver–bromide complex forms a stable surfactant bilayer strongly adsorbed on the gold surface, which binds to particular faces of Au crystal. Thus, there is a prevent of the growth on these faces, leading to elongation of the crystal. The second mechanism assumes that Ag^+ ions change the shape of CTAB micelles, from spherical to cylindrical, directing the formation to Au nanorods. Finally, the third mechanism was proposed by Liu and Guyot-Sionnest, suggesting that underpotential deposition (UPD) of Ag(0) occur at different Au faces leading to symmetry-breaking and thus, the rod formation [38]. Underpotential deposition is a process that occurs through the formation of a metal adlayer onto a more noble metal substrate. That is, when a metal substrate is cathodically polarized, ions of a less noble metal can be deposited coating the substrate [39]. Specifically, the stabilization of an adsorbate layer is higher when the substrate has open facets. Because of this, the reduction of Ag adatoms on gold occur preferentially on the higher energy crystal facets with more atoms to be coordinated, i.e., [110] facets, followed by [100] and [111] facets, respectively. It assumes that Ag adatoms act as strong binding agent on longitudinal [110] facets, leading to one-dimensional growth along [100] direction [35,40]. In this work, we adopted the model proposed by Liu and Guyot-Sionnest to analyse and discuss the binding energies observed by XPS and to carried out *ab initio* simulations.

Fig. 2a–f show the high-resolution spectra of the constituents of the gold nanorods. Fig. 2a shows the C 1s spectrum that was deconvoluted into four components. The most intense C 1s signal identified as C1 corresponding to carbon bound to carbon or hydrogen at 284.8 eV, derived from the aliphatic chain of CTAB. As aforementioned, all other values of binding energy have been referenced for that specific component. The first remark indicates a large percentage of aliphatic carbon (63.2%), even after washed away part of CTAB molecules in the preparation step. The signal at 285.6 eV identified as C2 was assigned to carbon bound to an amine [41]. These observations are consistent with previous reports that C 1s can be resolved in two main components corresponding to C–C and C–N bonding [42]. Important to notice that the atomic ratio C1/N = 63.19/3.77 = 16.8 is close to the atomic ratio C1/N = 15 of the alkane chain and nitrogen of CTAB. The concentration of the second observed carbon C2 is 19.6% and its ratio C2/N = 19.64/3.77 = 5.21, nearly to the atomic ratio of de CTAB head charged group (4C/1N = 4). Finally, the components at higher energy C3 and C4 were ascribed to carbon bound to nitrogen ($H_3\underline{C}$–N–C) at 286.3 eV and a weak component near 287.8 eV attributed to adventitious carbon ($\underline{C}_{adv}$ = O) or amide group [41,43,44].

The N1s spectrum (Fig. 2b) was fitted in one component at 402.1 eV and that was ascribed to the protonated amine of the surfactant head-group [45,46]. Bromine presented a doublet peak corresponding to $3d_{5/2}$ and $3d_{3/2}$ at 67.0 and 68.1 eV,

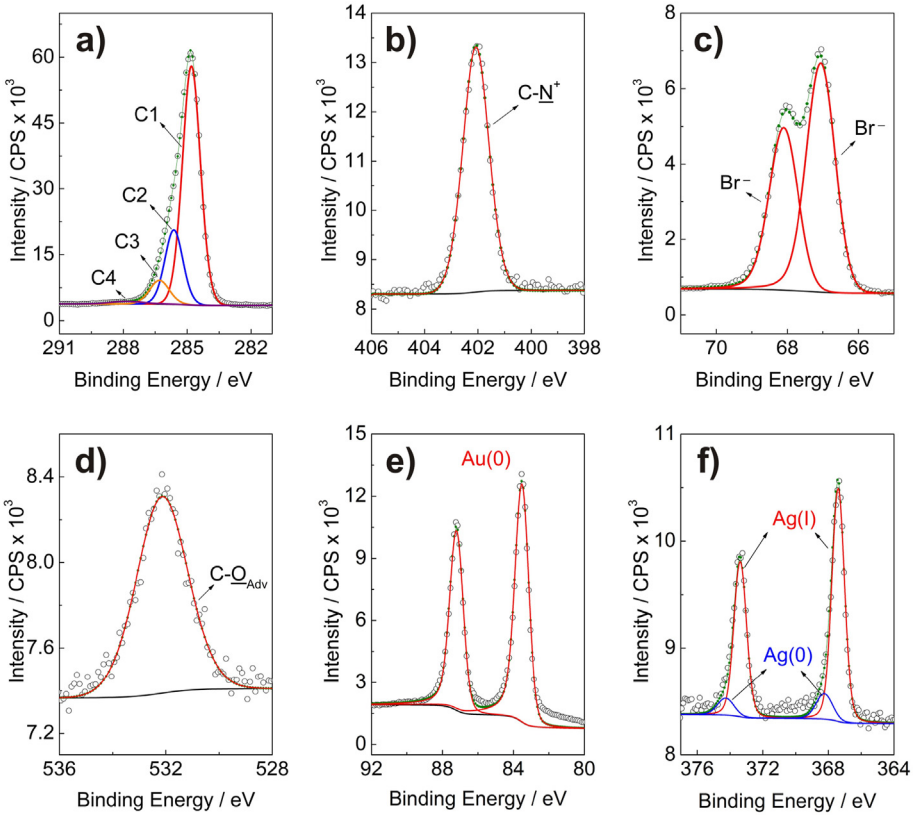

Fig. 2 – Deconvolution of high-resolution spectra of the elements in the regions (a) C 1s, (b) N 1s, (c) Br 3d, (d) O 1s, (e) Au 4f and (f) Ag 3d. Open circles represent the CPS signal while the green line is the envelope.

respectively (Fig. 2c) that can be associated to the bromide anion in CTAB [45]. The O1s spectrum shown in Fig. 2d was resolved in one component at 532.1 eV attributed to oxygen bound to nitrogenated carbon.

The high-resolution gold spectrum in the Au 4f region is shown in Fig. 2 (e). The Au $4f_{7/2}$ photoelectron peak is located at 83.5 eV and $4f_{5/2}$ is located at 87.2 eV. Other experimental parameters such as FWHM and spin-orbit split presented values of 0.94 eV and $\Delta = 3.7$ eV. These binding energy values are smaller than 84.0 eV and 87.0 eV for the Au $4f_{7/2}$ and Au $4f_{5/2}$, respectively, usually ascribed to zerovalent gold [47]. From a chemical perspective, the origin of these BE at lower energies could be evidence of the interaction of surface gold with different species (bromide anion, CTA^+ and silver) accommodated on the crystal surface [41].

To gain insight into the chemical state of components in the metallic core, we carried out computation experiments to estimate the binding energies through the Slater transition state with the WIEN2k package. The starting structure considered for computation correspond to the bulk fcc Au crystal. Initially, it was calculated the binding energy of Au crystal, which presented the following values: 83.4 and 87.4 eV for the doublets $4f_{7/2}$ and $4f_{5/2}$, respectively. As can be seen in Table 2, theoretical binding energies are in excellent agreement with experimental data obtained by XPS (i.e., 83.5 and 87.2 eV for the same Au 4f doublets) even bear in mind that calculations were done considering Au bulk crystal and ignoring the interactions with CTAB.

Our experimental results for the binding energy of silver indicate the presence of two components, as shown in Fig. 2f. The figure shows the XPS Ag 3d spectrum and the curve fitting presents characteristic Ag $3d_{5/2}$ and Ag $3d_{3/2}$ peaks at 367.4 eV and 373.4 eV, respectively. Similar values were observed by other research groups that attributed this particular energy to the Ag(I) species [34]. Furthermore, in addition to Ag(I) contribution, one additional doublet is necessary to fit the envelope curve: a second Ag chemical state with Ag $3d_{5/2}$ and Ag $3d_{3/2}$ peaks at 368.2 eV and 374.3 eV, respectively, attributed to zerovalent silver (Ag(0)) [48,49]. The most significant feature in the Ag 3d spectrum is the large difference in the concentration between two silver species in the nanorods: Ag(I) comprises 85.7% of the total silver signal while Ag(0) comprises 14.3%, respectively. Based on the XPS results for Ag(0), we decide to model some configurations of silver atoms on a gold crystal. Firstly, the binding energy of Ag adatom on an Au [111] crystal was computed, and the values obtained were 365.5 and 372.0 eV for the Ag $3d_{5/2}$ and Ag $3d_{3/2}$, respectively (Table 2). These values are approximately 1.9 eV smaller than experimental Ag(0) doublet (i.e., 368.2 and 374.3 eV), which is quite reliable since we do not consider any chemical interactions with CTAB. It should be mentioned that the binding energy of the core electrons usually increases when the valence electrons are involved in bonds (such as Ag and bromide bonds in the Au-NRs) and, therefore, it is expected that BE obtained from theory is smaller than experimental XPS [50].

In the case of Ag located in the inner of Au-NRs, knowledge of different chemical configurations is a critical issue because this information is not available through experimental XPS. Therefore, calculations were performed to estimate the binding energy of the Ag atoms in the inner of Au-NRs. As mentioned in the previous section, the chemical state of silver in Au-NRs remains unclear and controversial. Moreau and co-workers recently reported a new model to explain the chemical state of silver in Au-NRs using a combination of spectroscopic techniques such as X-ray absorption fine structure (XAFS), X-ray fluorescence (XRF), and EDX-mapping [15]. In accord with the authors, silver atoms are reduced by under-potential deposition (UPD) on the surface of Au nanoparticles in the very early stages of nanorods formation. During the step of anisotropic growth of nanoparticles, Ag(0) adsorbs onto nanoparticles surface stabilizing the [110] facets, which leads to an elongation of nanoparticles with preferential reduction of Au in the rod extremities. With the progress of reaction time, Ag is incorporated to nanorod inner due to subsequent deposition of Au atoms until reaction completion (approximately 120 min). In our simulation, we assume the presence of Ag as substitutional (i.e., Ag-on-Au site) and interstitial defects in the crystalline lattice of gold. Our theoretical studies revealed that Ag-on-Au sites are more energetically favorable than interstitial Ag in the gold crystal because the defect formation energy (that is, the difference between the formation energy of an ideal crystal and a defective one) is 0.6 eV higher in crystals with interstitial defects (check Fig. S1a and b at ESI for details). This mean that the interstitial Ag forces a disturbance on the gold lattice, while substitutional Ag has almost no effect, as expected since the two atom types have very similar atomic radii. Therefore, from the defect formation energy data, interstitial Ag is not expected in Au crystals. The calculated binding energy for Ag 3d substitutional was 365.8 and 372.2 eV for $3d_{5/2}$ and $3d_{3/2}$, respectively (see Table 2). Also, the calculated binding energy for Ag 3d interstitial was found at 366.5 and 372.8 eV for $3d_{5/2}$ and $3d_{3/2}$, respectively. Unfortunately, no experimental data are available to compare to these theoretical values of binding energy because the information of a typical layer thickness measured by XPS is around 5–10 nm [32]. Thus, also considering the surfactant bilayer, XPS is not appropriate to infer whether Ag atoms are, in fact, spread to

Table 2 – XPS parameters of zerovalent metallic elements in Au-NRs in eV as obtained by experiments and *ab initio* calculations.

	Experimental	Theory
Au 4f doublets		
BE (eV)	83.5, 87.2	83.4, 87.4
FWHM (eV)	0.94	–
Spin-Orbit Split (eV)	3.7	4.0
Ag 3d doublets		
BE (eV)	368.2, 374.3	365.5, 372.0 (surface) 366.5, 372.8 (interstitial) 365.8, 372.2 (substitutional)
FWHM (eV)	1.01	–
Spin-orbit split (eV)	6.0	6.5 (surface) 6.3 (interstitial) 6.4 (substitutional)

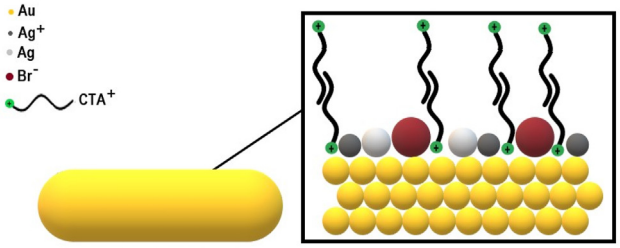

Scheme 1 – Schematic representation of an isolated Au-NR and details of its outermost surface after washing with diluted CTAB solution in air. Adventitious carbon ($C_{adv} = O$) species are not shown in this model.

the bulk of Au-NRs and we cannot test the hypothesis of Moreau and co-workers.

Consequently, our experiments lead us to conclude that the two-chemical state for silver may be in accordance with the hypothesis proposed by Ye and co-workers to explain the oxidation of Ag(0) monolayer over Au-NRs [16]. In this paper, the authors detected the presence of a silver surface layer on Au-NRs. Monitoring the evolution of the plasmon scattering signal, they noticed that the washing of CTAB from gold rods, the silver layer initially protected by the surfactant CTAB, gets oxidized as soon as CTAB desorbs due to a reduced concentration in the flowing solution. In our experiments, it was necessary to remove the excess surfactant from the Au-NRs by washing the samples with a more diluted CTAB solution to perform the XPS measurements. Therefore, during the process of washing and handling of Au-NRs on-air, may be occurred the oxidation of the Ag atoms on the crystal surface as shown in the reactions below: [51,52].

$$2Ag^0 + \frac{1}{2}O_2 \leftrightharpoons Ag_2O \quad (1)$$

$$Ag_2O + 2H^+ \rightleftharpoons 2Ag^+ + H_2O \quad (2)$$

Since it was detected two chemical states for Ag, we assume that this washing procedure may also lead to an oxidation process of the silver layer, generating a mixing Ag(0) and Ag(I) species on the gold surface, as can be visualized in Scheme 1.

4. Conclusion

In summary, we studied the outermost layer of Au-NRs using XPS spectroscopy and *ab initio* calculations in order to get insights regarding the chemical states of the constituents of the metallic core. Three significant results can be extracted from this paper. First, *ab initio* simulations showed that Ag atoms might have different binding energies, depending on the configuration of silver atoms in Au-NRs. Second, our XPS results indicate the presence of a mixed Ag(0)/Ag(I) species on the surface of Au-NRs, corroborating with recent results in the literature that shows that Ag(0) monolayer can be oxidized to Ag(I) during the steps of centrifugation and washing with diluted CTAB solution. Finally, our theoretical studies showed that silver atoms located at interstitial sites could distort the crystalline structure, and, therefore, this defect should be unlikely to occur in Au-NRs. That is, an interstitial position would imply a rather large relaxation and make the Au-NR more unstable at high Ag concentrations.

Author contributions

C. Oliveira performed the synthesis experiments. C. Oliveira and P. Bargiela performed the XPS experiments. C. R. Chaves helped in the stages of synthesis and characterization by TEM. C. Persson performed the DFT calculations. C. Oliveira, M.G.M.C. Rocha, J.F.D. Chubaci, M. Boström, A. F. Silva, C. Persson, and M. Malta analyzed the data. A. F. Silva, C. Persson, and M. Malta designed the study. C. Persson and M. Malta wrote the manuscript. All authors have approved the final version of the manuscript.

Declaration of Competing Interest

The authors declare that they have no known competing financial interests or personal relationships that could have appeared to influence the work reported in this paper.

Acknowledgments

The authors thank the funding agencies Capes, Fapesb/CNPq (Pronem: PNE0012/2011, Pronex: PNX0007/2011 and INT0003/2015), CNPq, RCN (project 251131), and Proc. USP 2019.1.971.43.0 for financial support. We would like to thank the technical staff of the CME/UFMG for the help with electronic microscopy characterizations during the execution of this work. Finally, we acknowledge the access to HPC resources provided by SNIC/Sweden and NOTUR/Norway.

Appendix A. Supplementary data

Supplementary data to this article can be found online at https://doi.org/10.1016/j.jmrt.2021.08.059.

REFERENCES

[1] Rajput S, Werezuk R, Lange RM, McDermott MT. Fungal isolate optimized for biogenesis of silver nanoparticles with enhanced colloidal stability. Langmuir 2016;32(34):8688–97.
[2] El-Sayed MA. Some interesting properties of metals confined in time and nanometer space of different shapes. Acc Chem Res 2001;34(4):257–64.
[3] Rossi LM, Fiorio JL, Garcia MAS, Ferraz CP. The role and fate of capping ligands in colloidally prepared metal nanoparticle catalysts. Dalton Trans 2018;47(17):5889–915.
[4] Grzelczak M, Vermant J, Furst EM, Liz-Marzan LM. Directed self-assembly of nanoparticles. ACS Nano 2010;4(7):3591–605.
[5] Jain PK, Huang XH, El-Sayed IH, El-Sayed MA. Noble metals on the nanoscale: optical and photothermal properties and some applications in imaging, sensing,

biology, and medicine. Acc Chem Res 2008;41(12):1578–86.
[6] Murphy CJ, Thompson LB, Alkilany AM, Sisco PN, Boulos SP, Sivapalan ST, et al. The many faces of gold nanorods. J Phys Chem Lett 2010;1(19):2867–75.
[7] Linic S, Christopher P, Ingram DB. Plasmonic-metal nanostructures for efficient conversion of solar to chemical energy. Nat Mater 2011;10(12):911–21.
[8] Cobley CM, Chen JY, Cho EC, Wang LV, Xia YN. Gold nanostructures: a class of multifunctional materials for biomedical applications. Chem Soc Rev 2011;40(1):44–56.
[9] Huang XH, Neretina S, El-Sayed MA. Gold nanorods: from synthesis and properties to biological and biomedical applications. Adv Mater 2009;21(48):4880–910.
[10] Merrill NA, Sethi M, Knecht MR. Structural and equilibrium effects of the surface passivant on the stability of Au nanorods. ACS Appl Mater Interfaces 2013;5(16):7906–14.
[11] Jia YP, Shi K, Liao JF, Peng JR, Hao Y, Qu Y, et al. Effects of cetyltrimethylammonium bromide on the toxicity of gold nanorods both in vitro and in vivo: molecular origin of cytotoxicity and inflammation. Small Methods 2020;4(3):11.
[12] Grabinski C, Schaeublin N, Wijaya A, D'Couto H, Baxamusa SH, Hamad-Schifferli K, et al. Effect of gold nanorod surface chemistry on cellular response. ACS Nano 2011;5(4):2870–9.
[13] Nikoobakht B, El-Sayed MA. Preparation and growth mechanism of gold nanorods (NRs) using seed-mediated growth method. Chem Mater 2003;15(10):1957–62.
[14] Almora-Barrios N, Novell-Leruth G, Whiting P, Liz-Marzan LM, Lopez N. Theoretical description of the role of halides, silver, and surfactants on the structure of gold nanorods. Nano Lett 2014;14(2):871–5.
[15] Moreau LM, Jones MR, Roth EW, Wu J, Kewalramani S, O'Brien MN, et al. The role of trace Ag in the synthesis of Au nanorods. Nanoscale 2019;11(24):11744–54.
[16] Ye WX, Kruger K, Sanchez-Iglesias A, Garcia I, Jia XY, Sutter J, et al. CTAB stabilizes silver on gold nanorods. Chem Mater 2020;32(4):1650–6.
[17] Hubert F, Testard F, Spalla O. Cetyltrimethylammonium bromide silver bromide complex as the capping agent of gold nanorods. Langmuir 2008;24(17):9219–22.
[18] Niidome Y, Nakamura Y, Honda K, Akiyama Y, Nishioka K, Kawasaki H, et al. Characterization of silver ions adsorbed on gold nanorods: surface analysis by using surface-assisted laser desorption/ionization time-of-flight mass spectrometry. Chem Commun 2009;(13):1754–6.
[19] Hostetler MJ, Wingate JE, Zhong CJ, Harris JE, Vachet RW, Clark MR, et al. Alkanethiolate gold cluster molecules with core diameters from 1.5 to 5.2 nm: core and monolayer properties as a function of core size. Langmuir 1998;14(1):17–30.
[20] Blaha P, Schwarz K, Madsen GKH, Kvasnicka D, Luitz J, Laskowski R, et al., WIEN2k. An augmented plane wave plus local orbitals program for calculating crystal properties techn. Universitat; 2018. p. 287.
[21] Kresse G, Furthmuller J. Efficiency of ab-initio total energy calculations for metals and semiconductors using a plane-wave basis set. Comput Mater Sci 1996;6(1):15–50.
[22] Kresse G, Joubert D. From ultrasoft pseudopotentials to the projector augmented-wave method. Phys Rev B 1999;59(3):1758–75.
[23] Jana NR, Gearheart L, Murphy CJ. Wet chemical synthesis of high aspect ratio cylindrical gold nanorods. J Phys Chem B 2001;105(19):4065–7.
[24] Jana NR, Gearheart L, Murphy CJ. Seed-mediated growth approach for shape-controlled synthesis of spheroidal and rod-like gold nanoparticles using a surfactant template. Adv Mater 2001;13(18):1389–93.
[25] Chen Y, Gu X, Nie CG, Jiang ZY, Xie ZX, Lin CJ. Shape controlled growth of gold nanoparticles by a solution synthesis. Chem Commun 2005;(33):4181–3.
[26] Personick ML, Langille MR, Zhang J, Mirkin CA. Shape control of gold nanoparticles by silver underpotential deposition. Nano Lett 2011;11(8):3394–8.
[27] Langille MR, Personick ML, Zhang J, Mirkin CA. Defining rules for the shape evolution of gold nanoparticles. J Am Chem Soc 2012;134(35):14542–54.
[28] Gonzalez-Rubio G, Kumar V, Llombart P, Diaz-Nunez P, Bladt E, Altantzis T, et al. Disconnecting symmetry breaking from seeded growth for the reproducible synthesis of high quality gold nanorods. ACS Nano 2019;13(4):4424–35.
[29] Link S, El-Sayed MA, Mohamed MB. Simulation of the optical absorption spectra of gold nanorods as a function of their aspect ratio and the effect of the medium dielectric constant (vol 103B, pg 3073, 1999). J Phys Chem B 2005;109(20):10531–2.
[30] Link S, Mohamed MB, El-Sayed MA. Simulation of the optical absorption spectra of gold nanorods as a function of their aspect ratio and the effect of the medium dielectric constant. J Phys Chem B 1999;103(16):3073–7.
[31] Yan BH, Yang Y, Wang YC. Comment on "Simulation of the optical absorption spectra of gold nanorods as a function of their aspect ratio and the effect of the medium dielectric constant". J Phys Chem B 2003;107(34):9159.
[32] Greczynski G, Hultman L. X-ray photoelectron spectroscopy: towards reliable binding energy referencing. Prog Mater Sci 2020;107.
[33] Tan SF, Raj S, Bisht G, Annadata HV, Nijhuis CA, Kral P, et al. Nanoparticle interactions guided by shape-dependent hydrophobic forces. Adv Mater 2018;30(16).
[34] Grzelczak M, Sanchez-Iglesias A, Rodriguez-Gonzalez B, Alvarez-Puebla R, Perez-Juste J, Liz-Marzan LM. Influence of iodide ions on the growth of gold nanorods: tuning tip curvature and surface plasmon resonance. Adv Funct Mater 2008;18(23):3780–6.
[35] Orendorff CJ, Murphy CJ. Quantitation of metal content in the silver-assisted growth of gold nanorods. J Phys Chem B 2006;110(9):3990–4.
[36] Scarabelli L, Sanchez-Iglesias A, Perez-Juste J, Liz-Marzan LM. A "tips and tricks" practical guide to the synthesis of gold nanorods. J Phys Chem Lett 2015;6(21):4270–9.
[37] Lohse SE, Murphy CJ. The quest for shape control: a history of gold nanorod synthesis. Chem Mater 2013;25(8):1250–61.
[38] Liu MZ, Guyot-Sionnest P. Mechanism of silver(I)-assisted growth of gold nanorods and bipyramids. J Phys Chem B 2005;109(47):22192–200.
[39] Grzelczak M, Perez-Juste J, Mulvaney P, Liz-Marzan LM. Shape control in gold nanoparticle synthesis. Chem Soc Rev 2008;37(9):1783–91.
[40] Murphy CJ, Thompson LB, Chernak DJ, Yang JA, Sivapalan ST, Boulos SP, et al. Gold nanorod crystal growth: from seed-mediated synthesis to nanoscale sculpting. Curr Opin Colloid Interface Sci 2011;16(2):128–34.
[41] del Cano R, Gisbert-Gonzalez JM, Gonzalez-Rodriguez J, Sanchez-Obrero G, Madueno R, Blazquez M, et al. Effective replacement of cetyltrimethylammonium bromide (CTAB) by mercaptoalkanoic acids on gold nanorod (AuNR) surfaces in aqueous solutions. Nanoscale 2020;12(2):658–68.
[42] Li YP, Yu HZ, Huang XX, Wu ZP, Xu HH. Improved performance for polymer solar cells using CTAB-modified MoO3 as an anode buffer layer. Sol Energy Mater Sol Cell 2017;171:72–84.
[43] Boufi S, Vilar MR, Ferraria AM, do Rego AMB. In situ photochemical generation of silver and gold nanoparticles

on chitosan. Colloid Surface Physicochem Eng Aspect 2013;439:151–8.
[44] Moulder JF, Stickle WF, Sobol PE, Bomben KD. Handbook of X-ray photoelectron spectroscopy. Eden Prairie, Minnesota: Physical Electronics Division, Perkin-Elmer Corporation; 1992.
[45] Ahmad R, Boubekeur-Lecaque L, Nguyen M, Lau-Truong S, Lamouri A, Decorse P, et al. Tailoring the surface chemistry of gold nanorods through Au-C/Ag-C covalent bonds using aryl diazonium salts. J Phys Chem C 2014;118(33):19098–105.
[46] Techane SD, Gamble LJ, Castner DG. X-ray photoelectron spectroscopy characterization of gold nanoparticles functionalized with amine-terminated alkanethiols. Biointerphases 2011;6(3):98–104.
[47] Fuggle JC, Martensson N. Core-level binding-energies in Metals. J Electron Spectrosc Relat Phenom 1980;21(3):275–81.
[48] Watanabe F, Nima ZA, Honda T, Mitsuhara M, Nishida M, Biris AS. X-ray photoelectron spectroscopy and transmission electron microscopy analysis of silver-coated gold nanorods designed for bionanotechnology applications. Nanotechnology 2017;28(2).
[49] Ke SL, Kan CX, Ni Y, Zhu XZ, Jiang MM, Wang CS, et al. Construction of silica-encapsulated gold-silver core-shell nanorod: atomic facets enrichment and plasmon enhanced catalytic activity with high stability and reusability. Mater Des 2019;177.
[50] Tardio S, Cumpson PJ. Practical estimation of XPS binding energies using widely available quantum chemistry software. Surf Interface Anal 2018;50(1):5–12.
[51] Xiu ZM, Zhang QB, Puppala HL, Colvin VL, Alvarez PJJ. Negligible particle-specific antibacterial activity of silver nanoparticles. Nano Lett 2012;12(8):4271–5.
[52] Liu JY, Hurt RH. Ion release kinetics and particle persistence in aqueous nano-silver colloids. Environ Sci Technol 2010;44(6):2169–75.